From micro to nano scales -recent progress in the characterization of nitrided austenitic stainless steels

LUO, Quanshun <http://orcid.org/0000-0003-4102-2129> and YANG, Shicai

SciForschen
Open HUB for Scientific Research

International Journal of Nanomedicine and Nanosurgery

Review Article | Volume: 1.1 | Open Access

From Micro to Nano Scales -Recent Progress in the Characterization of Nitrided Austenitic Stainless Steels

Quanshun Luo[1]* and Shicai Yang[2]

[1]*Materials and Engineering Research Institute, Sheffield Hallam University, Howard Street, Sheffield S1 1WB, UK*
[2]*Teer Coatings Ltd, Miba Coating Group, West Stone House, Berry Hill Industrial Estate, Droitwich, WR9 9AS, UK*

***Corresponding author:** Quanshun Luo, Materials and Engineering Research Institute, Sheffield Hallam University, Howard Street, Sheffield S1 1WB, UK, **E-mail:** q.luo@shu.ac.uk

Received date: 03 March 2015; **Accepted date:** 03 April 2015; **Published date:** 08 April 2015.

Citation: Luo Q, Yang S (2015) From Micro to Nano Scales -Recent Progress in the Characterization of Nitrided Austenitic Stainless Steels. J Nanomed Nanosurg, Volume1.1: http://dx.doi.org/10.16966/ijnn.101

Abstract

In the frontier of materials science, understanding of materials has been in multiple scales from macro, micro, to atomic levels. This is attributed to the advanced instrumentations such as SEM, TEM, XPS, XRD, as well as several other spectroscopic and metallographic analyses. Fe-Cr-Ni based austenitic stainless steels have a diverse range of modern applications ranging from biomedical prostheses in human bodies, food processing, to chemical engineering and nuclear power generation. The outstanding properties of the nitrided steels have attracted extensive research activities attempting to obtain a clear image on the structural characteristics of the structure, including nano-scale heterogeneity of the expanded austenite phase resulted from atomic-level chemical or electronic interactions in the alloying system. This paper provides a review on the structural characterization of nitrided austenitic stainless steels, with an emphasis on the latest experimental findings through the use of these sophisticated analytical tools. In the final section, several possible aspects of future studies are discussed.

Keywords: Stainless steel; Nitriding; Electron sicroscopy; X-ray diffraction; Spectroscopic analysis; Characterization techniques

Introduction

Austenitic stainless steel attracts wide applications for biomedical implants, medical devices, and pharmaceutical processes, because it is biomedically compatible, hygienic, corrosion resistant, easy to clean, and of low life-cycle costs [1-3]. As a class of iron based Fe-Cr-Ni ternary alloys, austenitic stainless steel has its principal physical and mechanical properties primarily from iron, whereas the chemical stability especially the anti-corrosion performance is owing to the chromium component which governs the kinetic process of the chemical degradation. Of course, nickel also plays an important role in stabilizing the austenitic phase and bringing about many other beneficial properties. According to the corrosion theory [4-6], austenitic stainless steel gains its extraordinary corrosion resistance in an oxidative medium owing to the immediate formation of a passive chromium oxide Cr_2O_3 film, which is chemically stable, structurally dense and therefore works as a barrier to greatly restrict further oxidation of the inner metallic matrix. Secondly, the high chromium content significantly increases the electrode potential of the ferrous matrix, leading to better resistance to electrochemical corrosion.

In the field of health and medical services, austenitic stainless steel forms a family of important structural materials for numerous medical and surgical implants, tools, devices and equipment. It is of great value to improve the corrosion resistance and life-cycle performance. However, a major drawback of austenitic stainless steel is the low hardness causing very poor resistance to scratching and abrasive wear. To overcome this, a surface nitriding treatment is applied to generate a nitrogen-rich surface layer of much higher hardness, which consequently reduces scratching damages and abrasive wear. Nitriding processes started from the conventional gaseous surface thermo-chemical treatment, whereas great achievements have been made in plasma enhanced nitriding technologies. In particular, perhaps the most striking technical innovation in this aspect was the development of low-temperature plasma nitriding treatments, which brought about the formation of a single phase layer of nitrogen super-saturated austenite-like structure free from nitride precipitates. Such a low-temperature nitriding process offers both excellent oxidation resistance, at least equivalent to the bare austenitic stainless steel, and extremely good anti-wear property. For the plasma nitriding of austenitic stainless steels, major research interests have been allocated in the chemical interactions between nitrogen and the Fe, Cr and Ni components, the diffusion kinetics of nitrogen atoms in the austenitic matrix, and structure of the nitrided layers.

In the structural characterization of low-temperature plasma nitrided austenitic stainless steels, breakthrough research has been reported beyond the aspects of crystallite grains, grain boundaries and lattice defects, in the attempts to understand the nitrided layers from the view of chemical bonding, atomic stacking structure and the interactions of valence electrons. These achievements resulted from the multidisciplinary nature of recent research, e.g., through the use of many advanced analytical tools, from electron microscope based secondary electron imaging, backscattered electron imaging, diffraction contrast (bright field and dark field) imaging, and phase contrast imaging, energy dispersive X-ray spectroscopic and electron energy loss spectroscopic analyses, to many other sophisticated microscopic, spectroscopic and diffractometric techniques. As a short review, this paper is only focused on selected readings of recent structural characterization, chemical and physical analyses of nitrided austenitic structure as well as the related plasma technology. In particular, most selected reference papers demonstrated comprehensive understanding of the nitrided structure depending on the employed instrumental techniques. Therefore, unlike many other reviews of similar scientific contents, we have structured the review in terms of the analytical means, e.g. from the very conventional analyses to the latest techniques. Although most initial experimental findings were evidenced in figures, curves, and tables, etc., the current review only provides a text based highlight of the findings in order to save space. However, we would recommend the relevant cited paper if one intends to find more details in any particular case. It is expected that this brief review could bring some indicative light to promote fundamental understanding of the nitride

structures, and could also be recommendable to the research in other surface engineering materials.

Technological Aspects of Plasma Nitriding Processes

Steel surface gas nitriding was primitively recognized by Machlet [7], who found that diffusion of nitrogen in iron or iron-based steels improved the surface properties in terms of high hardness, fatigue and wear resistance. Pye illustrated an iron-nitrogen equilibrium phase diagram to explain the solubility of nitrogen in iron at temperature range from 480 to 680°C in which various phases of α-Fe, γ-Fe, or ε-Fe(N) were formed depending on an equilibrium temperature[8].

Early gas nitriding processes of steels were in principal similar to those reported in[7], where nitriding was performed in ammonia or ammonia with addition of hydrogen mixture in a vacuum chamber [9,10]. The nitrogen atoms were firstly dissociated from ammonia (NH_3) at elevated temperature and transported to surfaces of those heated steel components. Thereafter a nitride layer could be produced with typical structures of a top compound layer dominated by ε-Fe_3N_{1+y} phase and an subsurface diffusion layer with mainly the γ-Fe_4N_{1-x} [11], in which the process temperature was described as a crucial parameter to control the formation of specific Fe-N phases according to Lehrer diagram of nitrogen activity vs. Temperature [12].

Traditional gas nitriding requires a high process temperature, e.g. 500°C or higher, in order to dissociate ammonia (NH_3) efficiently and to make those nitrogen atoms diffuse into the steel surface. This is obviously a disadvantage because high temperature leads to increased thermal expansion and would cause distortion of the treated steel parts. In addition, industrial gas nitriding has to concern problems arising from the use of ammonia, including the corrosion induced leaking of the steel based ammonia container and the generation of large amount of flammable hydrogen accompanying the decomposition of ammonia ($NH_3 \rightarrow [N] + 3/2H_2$).

Plasma nitriding is in principal still a 'gaseous' process. Unlike the traditional gaseous nitriding, however, it employs glow discharge plasma which can efficiently dissociate the gaseous atoms at a very low process temperature, e.g. high rate dissociation of nitrogen atoms from N_2 glow discharge at gas temperature lower than 200°C as reported by Guerra [13]. Meanwhile, glow discharge plasma can effectively heat up the steel surface due to those energetic particles in plasma, which improves the diffusion or penetration of N atoms into the steel matrix. Berghaus exploited electric glow discharge technique for a nitriding process, in which glow discharged mixture of N_2 and H_2 was employed to heat up the steel and, at the same time, nitriding took place inside a steel gun tube to increase the hardness and wear resistance of the internal surface [14].

The conventional dc plasma nitriding was relied on bombarding by energetic particles in a gaseous glow discharge process. An industrial dc plasma process can be described according to a schematic diagram shown in Figure1, in which Ar or H_2+N_2 plasma is produced by a dc power unit. Through the applied high negative bias voltages, the steel parts for nitriding are immersed in the plasma with ion sheath (known as Child–Langmuir (CL) sheath) formed around surfaces of each individual parts and there is also an anode dark space close to chamber wall. In such a system, bombarding of energetic particles is critical to control uniform nitriding.

The treated parts can be treated as multiple cathodes that should be operated in abnormal glow discharge (as described in voltage-current diagram of Townsend glow discharge) so the plasma glow can fully cover all the surfaces of the parts to make uniform plasma surface treatment. If the parts are different in size or the distances of the parts are not the same from parts to anode wall, then the abnormal glow is difficult to form with

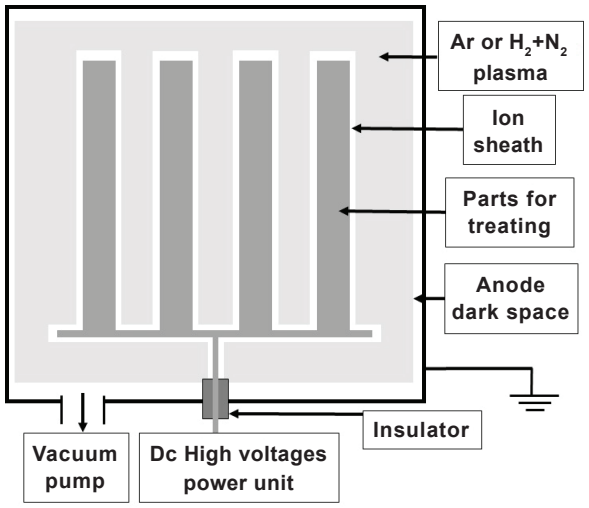

Figure 1: Schematic diagram of an industrial dc plasma nitriding process.

uniform coverage on surfaces of the all parts because the characterisations of a glow discharge plasma are dependent on gaseous pressure as well as the size and distance of the separated cathodes. Glow discharges at some surfaces of the parts (especially small parts and parts with sharp edges, or parts with different surface contaminations) may go rapidly transition from glow to arc discharge that would cause damages on the surfaces of treated parts and it is in general very difficult to make a uniform plasma nitriding economically for industrial applications.

A significant improvement of industrial plasma nitriding process, known as active screen plasma nitriding, was made by Georges [15], in which a metal screen cage covering the parts under nitriding is biased by either a dc or pulsed high negative voltage whilst the parts are just floated or weakly biased by a low voltage. In this process, the cage serves as a main cathode to produce high dense plasma, which in turn heat up the steel cage to reach high temperature due to intensive ion bombardment. The parts are then immersed in the plasma and heated up due to thermal radiation. Active screen plasma nitriding process has been now widely interested for industrial applications to treat various types of steel component [16].

Thermodynamics and Kinetics in Nitrided Structure Formation

Thermodynamics of a nitriding process

The thermodynamic system of steel under nitriding includes the steel itself and the nitriding atmosphere surrounding it. As a high potential of nitrogen is generated in the nitriding atmosphere in the form of mono-atomic nitrogen species in gas nitriding or energetic nitrogen ions in plasma nitriding, the nitrogen species are motivated to immigrate into the steel in order to make the entropy of the whole system higher. When the inter-atomic interactions between nitrogen and the metallic atoms in the steel are considered, one has to take account both the occupation of nitrogen atoms in the steel crystalline lattice and the ionic bonds between nitrogen and the metal atoms. In other words, nitrogen exists in the structure of austenitic stainless steel either as an interstitial solute to dissolve in the austenite matrix or in a metal nitride phase.

For the former, the atomic radius of nitrogen, 0.056 nm, is only slightly bigger than the radius of the γ-Fe octagonal vacancy (0.053 nm). This allows the formation of interstitial solid solution of high nitrogen content. Nitrogen has been reported to strongly stabilize the austenite phase by prohibiting the cementite precipitation and preventing austenite

to ferrite transformation. In brief, super saturation of nitrogen results in remarkable expansion of the austenite lattice, which has been evidenced by numerous results of X-ray diffraction experiments. Nitrogen alloyed austenitic stainless steels were reported to show increased strength and fatigue lifetime [6,17]. It also improves the corrosion resistance regarding localised pitting, crevice corrosion, inter granular corrosion, and the stress corrosion cracking failure [6,18-23]. These advantages are especially promising if the low hardness and or the weak corrosion resistance of austenitic steels are concerned, e.g. for some load-bearing parts working in a Cl-ion rich chemical environments.

For the latter, nitrogen as the 7th element in the chemical periodic table has five free electrons in its outer shell, and therefore intends to attract free electrons of chromium and iron to form chromium nitride and iron nitride. This behaviour dominates the nitride layers, which is to be discussed in details below, e.g. the stronger Cr-N bonds than the Fe-N and Ni-N.

Kinetic growth of nitriding layer

In a nitriding process, a case depth of nitrogen-rich surface layer is formed either as a supersaturated austenitic solid solution, known as expanded austenite γ_N (or S-phase as called by some authors [24,25]), or a compound layer dominated by chromium nitride, or a mixture of nitride precipitates dispersed in a ferrite matrix. A recent review paper has provided systematic description of the expanded austenite phase [25]. Moreover, the expanded austenite phase has been found to be heterogeneous in nano-scale because of the preferential Cr-N and Fe-N bondings. When the kinetic condition is met, the inward nitrogen atoms or ions combine preferentially to chromium to form chromium nitride compound, either as fine precipitates or in large grain sizes. This results in precipitation hardening or strengthening of the nitride layer, but also triggers the loss of corrosion resistance due to the reduced chromium concentration in the matrix or even the formation of ferrite phase.

Experimental measurements of the nitrogen concentration depth profiles contribute to understanding of the thermodynamics and kinetics of a nitriding process. Several sputtering based spectroscopic analyses are available to measure the concentration and depth profile of nitrogen in nitrided surfaces, including Auger electron spectroscopy (AES) [26-28], Glow discharge optical emission spectroscopy (GDOES) [29-34], secondary ion mass spectroscopy (SIMS) [35], and nuclear reaction analysis [32, 36]. As an example, Wu et al. employed Auger electron spectroscopy to analyse the depth profiles of nitrogen concentration of AISI 316L steel sample which were gas-nitrided for 20 hours at different temperatures of 350°C, 420°C, 440°C and 450°C [28]. On the 350°C nitrided surface, the maximum nitrogen concentration was approximately 15% with a very small nitrogen penetration depth less than 1 μm. The nitrogen penetration depth increased to 5 μm, 8 μm and 15 μm when the nitriding temperature was increased to 420°C, 440°C and 450°C, meanwhile the nitrogen concentration was also increased to 17% at the highest nitriding temperature. In addition to these profiling methods, energy dispersive X-ray (EDX) spectroscopy has been utilized to measure the nitrogen depth profile when working along with an analytical scanning electron microscopy (SEM) on a cross-section of nitride steel [37]. Figure 2 shows such a cross-sectional EDX profile of nitrided AISI 316 steel, noting the maximum nitrogen concentration at the surface as compared to the decreasing concentration towards the interface.

The kinetic process of surface nitriding treatment can be described as following. A nitrogen-rich media is provided inside a nitriding chamber, either in a gaseous or salt-bathing media, or in a plasma enhanced environment. The nitrogen atoms are chemically absorbed on the steel surface and subsequently penetrate into the austenite lattice by entering the octagonal vacancies. In many cases, a thin layer of chromium-iron

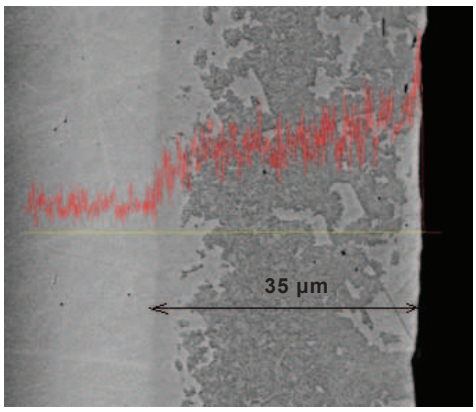

Figure 2: SEM-EDX linear profile of N-Kα in a polished cross-section of plasma nitride AISI 316 steel. The backscattered image indicates the thickness of the nitride layer to be 35 μm.

nitride compound is formed as a result of the absorption [11,33,38,39]. Then with increasing time at a certain temperature, anitrogen-enriched layer is formed and followed by the nitriding penetration.

Two modes have been proposed to describe the nitriding penetration, namely the diffusion driven mode and the trapping-detrapping mode.

The concentration dependent diffusion mode considers that, the inward diffusion is thermodynamically driven by the concentration gradient of nitrogen along the depth direction. Whereas nitrogen atoms occupy the octagonal vacancies of the f.c.c. lattice, the diffusivity obeys the related diffusion kinetics of interstitial atoms in f.c.c. metals. For example, the diffusion coefficient D_0 and activation energy Q of nitrogen in austenite are 3.3×10^{-6} $m^2 \cdot s^{-1}$ and 144×10^3 $J \cdot mol^{-1}$ respectively, comparing to the corresponding values of $4.6 \times 10^{-6} m^2 \cdot s^{-1}$ and 75×10^3 $J \cdot mol^{-1}$ for the diffusion of nitrogen in ferrite [40]. Mandl and Rauschenbach reported that, nitrogen plasma immersion ion implantation of austenitic stainless steel is characterised by a high nitrogen content of up to 20% [41]. The concentration dependent diffusion coefficients were calculated to explain the unusual fast diffusion. Christiansen and Somers reported numerical simulation and experimental measurement of concentration dependent diffusion coefficient of nitrogen in expanded austenite through the conduction of a denitriding experiment of thin initially N-saturated coupons in a gas mixture of ammonia and hydrogen [42]. Using the reported methods, they found an accurate approximation of the actual diffusivity of nitrogen in expanded austenite.

The trapping-detrapping mode derived from the different outer shell electronic statues of the three major metal components of austenitic stainless steels, and states that nitrogen atoms intend to bond preferentially to the Cr atoms because of stronger N-Cr chemical bond than the N-Fe and Ni-N bonds [33,43,44]. Then the diffusion under the influence of dynamic trapping and detrapping of inward nitrogen atoms controls the increase of the nitrided depth. The diffusion and detrapping activation energies of nitrogen in austenite stainless steel at around 400°C were reported to be 1.1 and 1.45 eV respectively, being in good agreement with experimental nitrogen profiles [43]. In another paper, Moskalioviene and co-workers reported that, the nitrogen detrapping activation energy is 0.28 eV, and the diffusion coefficient and the diffusion pre-exponential factor at 400°C are $4.80 \times 10^{-12} m^2 \cdot s^{-1}$ and 0.837×10^{-3} $m^2 \cdot s^{-1}$ respectively [33].

Influence of processing parameters on the kinetics of plasma nitriding

The kinetic growth of nitride layer is influenced by temperature and by the applied nitriding potential parameters, including the nitrogen partial

pressure in gaseous nitriding and the energetic nitrogen ion flux in plasma nitriding. Wu et al. reported that, the depth of nitrogen-enriched layer of gas-nitrided austenitic stainless steel (ALSI 316L) increased with the increase in the process temperature, the nitriding time, or the nitrogen activity coefficient [28].

For the influence of temperature, Zhang and Bell reported that, if the nitriding treatment is conducted at a moderate temperature lower than 450°C, a single phase layer of expanded austenite is formed [45]. On the other hand, plasma nitriding of Cr-Ni austenitic steel at 535°C-785°C resulted in a multi-phase nitrided layer (including ferromagnetic ferrite and CrN nitride) [46], which subsequent decreased in corrosion resistance despite the increased wear resistance.

Moller found that, in plasma nitriding of an austenitic stainless steel which naturally has a thin but dense Cr_2O_3-type oxide film on its surface, efficient nitriding required the transmission of the implanted ions through a surface oxide layer [44]. A balance is achieved between ion sputtering and re-oxidation from the residual gas for ion energies of certain plasma and gaseous conditions. In many cases, a gradient of nitrogen concentration can be obtained from the surface to certain depth. Lei reported that, in plasma nitrogen ion implantation, a nitriding case layer obtained at 380°C and 0.63 mA·cm^{-2} showed a maximum nitrogen concentration of 32 at% in a depth of approximately 2 μm, followed by a gradual decrease of the N concentration in the following depth [27]. The nitriding case depths increased from 1 μm, 12 μm to 17 μm when the nitriding temperature was increased from less than 300°C to the 380°C and 460°C. In addition, the applied N ion flux rate showed more pronounced influence on the penetration depth and the peak concentration at low process temperature, e.g. increase of the case depth from 1 μm to 5 μm and the maximum nitrogen concentration from 22 at% to 32 at% when the nitrogen dos rate was increased from 0.44 to 0.63 mA·cm^{-2}. Similar gradients of decreasing nitrogen concentration have also been reported by other researchers [33,36,37]. Asgari et al. measured the nitrogen concentrations at different depths of pulsed plasma nitride 316L stainless steel, and found decreased nitrogen concentration from 23.35% at the as-nitrided surface to 17.71 and 15.47 at% after 3 and 15 seconds of electro-polishing respectively. The enriched nitrogen concentration was associated with the formation of a single-phase expanded austenite with a lattice expansion of 5-12% for N=10-20 at%, and high indentation hardness of 8-10 GPa. Meanwhile, a cross-sectional linear scanning energy dispersive X-ray spectroscopy showed a profile of nitrogen concentration in a total depth of approximately 9 μm [37].

Structural Characterizations of Nitrided Austenitic Stainless Steel

Despite its very small thickness, a nitrided surface layer is extremely rich in structural characteristics, having extremely complicated structure. In particular, the obtained expanded austenite is thermodynamically meta-stable, supersaturated with interstitial nitrogen, precipitate-free but containing Cr-N and other short-range atomic orders. Understanding of the structural features has been attributed to the scientific and technical advances of materials characterization instruments. It is only by means of multi-disciplinary analytical research that the chemical, crystallographic and metallographic nature of the nitride layers could be understood. On the other hand, each employed analytical method can only provide a view of the analysed object in a selected window.

A typical example of such multi-technical experimental research can be found in the publications of Martinavicius and co-workers. In Ref. [36], the authors investigated the structure of a low temperature nitrided layer using a package of analytical tools including XRD, GDOES, field emission microscopy, conversion electron Mossbauer, X-ray absorption near edge structure and extended X-ray absorption fine structure spectroscopes. They found that the XRD homogeneous expanded austenite phase is microscopically heterogeneous because of the different local chemical environments of the Fe, Cr and Ni components. It consists of nanometric CrN precipitates dispersed in an N-saturated Fe_4N-like matrix. In their latest paper [47], a new instrumental technique, atomic probe tomography (APT) was employed to investigate the nano-scale heterogeneous distribution of Cr in a layer of expanded austenite. In the expanded austenite region studied, approximately 65 at% of Cr is detected as CrN^{2+} molecular ions, indicating interstitial-substitutional Cr-N bonds and the existence of CrN-like precipitates. Cr-N enriched bands, separating from each other at a distance of approximately 4.5 nm, were found to have 34.4 at% N, 30.8 at% Cr and only 3.6 at% Ni imaged along with Cr-depleted regions having average distances of ~4.5 nm. Between the Cr-N rich bands, the Cr and N are depleting (17.1 at% and 20.6 at% respectively) and would form Fe_4N as the local environment of Fe is very similar to γ'-Fe_4N. Therefore, the content of this chapter is arranged according to the characterization techniques.

Structural characterizations by indentation techniques

The most straight forward characterization of nitrided surfaces is micro hardness testing and the depth-sensitive nanoindentation. Whereas the former can be applied to determine the nitriding induced surface hardening [31,48-51] and the depth profile of hardness in the nitride cross-sections [51,52], the latter is also capable of measuring the elastic modulus [53,54]. Figure 3 shows the depth profiles of Knoop micro-hardness of plasma nitrided AISI 316 steel samples out of the authors' recent research. More results from published papers are described below.

Yasumaru et al. measured hardness of HV 1500 of AISI 304 austenitic stainless steel in a nitrided depth of 15μm as compared to the soft austenitic matrix of HV 300 [55]. In Ref. [56], AISI 316L austenitic stainless steel was nitrided through intensified plasma-assisted nitriding processes under a range of bias voltages 500V- 2,000V, cathode current densities 0.75 - 2.5 mA·cm^{-2} and the associated temperature measured from 400 to 750°C, which resulted in increased surface hardness from $HK_{0.1}$ 285 of the un-nitrided steel to $HK_{0.1}$ 930 - 2250 depending on the process conditions. On the sample nitrided at 400°C, nano-indentation determined a maximum hardness value over 15 GPa at the depth of ~4 μm, which gradually

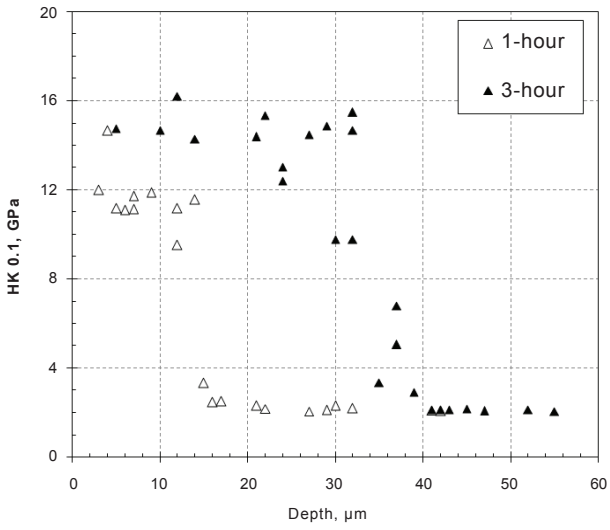

Figure 3: Knoop hardness of plasma nitrided AISI 316 steels, on metallographically polished cross-sections, indenting load 10 g. Note the increased depth of hardened layer and the increased hardness values after longer-time nitriding.

dropped to about 5 GPa at the depth of 12 μm approaching the hardness of the austenitic matrix. Meanwhile, the measured Young's modulus seemed to be independent of the depth position, ranging between 225 and 300 GPa due to data scattering. Fossati et al measured the surface microhardness values of $HK_{0.1}$ 1300-1605 on glow-discharge nitrided AISI 316L stainless steel samples accompanying the increase in nitriding temperature from 703K to 773K and the associated increase in the nitrides layer thickness from 10 to 47 μm [49].

Wang et al. found that, the case depth of DC plasma nitrided AISI 304 steel increased almost linearly from 5 to 12 μm along the increase of nitriding temperature from 350 to 500°C, whereas the maximum hardness ($HV_{0.1}$ 1000-1200) was obtained at the nitriding temperature 460°C [57]. Stinville et al. developed a technique of 2-D nano-indentation matrix measurements, SEM EBSD imaging and stress-less electro-polishing, to measure the 3D anisotropic changes in hardness and elastic modulus of plasma nitride 316L polycrystalline stainless steel and found that, the E modulus and hardness measured on individual grains depend strongly on their crystalline orientations [53,54]. The E modulus and hardness values of the nitride steel were 220-240 GPa and 13-16 GPa respectively depending on the crystalline orientation, comparing to the E modulus (190-215 GPa) and hardness (1.8 - 2.2 GPa) of the un-nitrided steel. In the samples prior to nitriding treatment, the <111> orientated grains showed the highest E modulus and hardness whereas those <001> oriented show the lowest. After plasma nitriding treatment, however, a reverse rank of the hardness and E modulus values was obtained, i.e. the <001> oriented grains showed the highest values and the <111> oriented the lowest.

In another paper, the nanoindentation determined E modulus was reported to be 162 GPa [58]. Asgari et al. measured a nano-indentation hardness profile obtained in a cross-section of an AISI 316L stainless steel being pulse plasma nitrided at a temperature lower than 440°C. The cross-sectional hardness values showed good correlation to the profile of nitrogen concentration [37].

Structural characterizations by optical microscopy

Optical microscopy has been widely applied to observe nitrided austenitic stainless steels, either on the changes in surface morphology due to anisotropic sputtering in plasma nitriding [52,55], or on the thickness and structural features on polished and chemically etched sections [30,31,49,50,55,59-61]. It has sufficient spatial resolution to image, on polished and chemically etched cross-sections; the nitrided layers provided that most of these layers are thicker than a few micrometers.

In addition, cross-sectional optical microscopy has been frequently employed to detect nitride precipitates within a nitrided case, in which the single phase of expanded austenite shows feature-less 'white' contrast because of its inertness to chemical etching and the areas of nitride precipitates always exhibit fine features of 'grey or black' contrast for the decreased resistance to the applied chemical etching. In Ref. [49], cross-sectional optical microscopy showed that the nitrided layer generated by glow discharge nitriding at 430°C was only 10 μm thick and exhibited feature-less white contrast indicating a single phase expanded austenite. In contrast, the 500 ^{0}Cnitrided layer was four times thicker and showed dispersed black features suggesting precipitation of nitrides. Similar application of cross-sectional optical microscopy was also included [51,61].

Furthermore, optical microscopy can provide more micro structural features if a cross-sectional sample is prepared in a small oblique angle, e.g. 5 degree [38]. On the oblique cross-sections, Sun and co-workers observed a very thin compound layer (γ'-Fe_4N, less than 0.5 μm thick) on the top of a nitrided 316 steel as well as fine precipitates at the expanded austenite grain boundaries. Similarly, such cross-sectional sample preparation was also applied in SEM observed samples of nitrided austenitic steel [62], in which the authors reported detailed observation of the interface, between the S-phase and the austenite substrate, as a narrow band of an unknown phase. This finding is interesting as in many optical microscopy observations, such interfaces (after chemical etching) are black lines. Perhaps more research is required to find details of this particular region.

Structural characterizations by analytical scanning electron microscopy

Comparing to optical microscopy, scanning electron microscopy has much more powerful spatial resolution. Meanwhile, advanced SEM instruments also work as a platform of chemical analyses by means of backscattered electron (BSE) imaging and energy dispersive X-ray (EDX) spectroscopic analysis, seeing (Figure 2) as an example. The material analysed in (Figure 2) is a high-power pulsed plasma nitrided austenitic stainless steel AISI 316. The cross-sectional SEM image was made at the BSE mode on a 6%-nital etched section to show the multi-phase structure of the nitrided layer. The EDX linear scan shows qualitatively the profile of nitrogen intensity (the characteristic X-ray N-K_a) in the whole thickness of the nitrided layer. In SEM imaging, the increased spatial resolution improves significantly the observations of nitriding induced surface morphological changes [48,55,56,61,63-66] and the cross-sectional structural features of nitrided cases [33-35,48,51,57,61-64,67-69]. More recently, a special SEM based diffractographic and metallographic technique, called electron backscattered diffraction (EBSD), has been introduced in structural characterization of nitride steels. EBSD technique is applied along with other analyses to investigate the anisotropic properties of polycrystalline austenitic steels [32,37,54,65,66].

In [32,65], SEM EBSD crystallographic imaging was applied to the surface of a 316L polycrystalline austenitic stainless steel before and after a plasma nitriding treatment. The nitrding treatment was found to lead to evolution of the orientation of the austenite grains, which favours enhanced <001> and <111> texture components. The orientation evolution was related to nitriding induced plastic deformation, e.g. high density slip bands observed on the nitride surface. In extreme case, short cracks were observed in some grains. Similar SEM-EBSD analysis was also reported [37], where the variation of crystalline orientation from the surface to different depth within a nitrided grain was claimed to be related to a gradient of nitrogen concentration. The nitrogen gradient was evidenced by a cross-sectional SEM-EDX line scan.

Cross-sectional SEM EBSD techniques have been applied to investigate the effect of the austenite crystalline orientation on the nitriding kinetics. In Ref.[66], SEM EBSD imaging showed that the local nitrogen penetration depth was not identical in different austenite grains. Similarly, Wu et al found that, the largest case depths were in the grains with their surface normal to a <100> direction and the smallest depths were in the grains of <111> direction [28].

Structural characterizations by X-ray diffraction

In 1986, Ichii reported in the first time an XRD pattern of low temperature (400°C) nitrided austenitic stainless steel, in which the five diffraction peaks detected were not listed in the ASTM index. Instead, the peaks shifted to lower angles with respect to the corresponding austenite peaks. Thereafter the unknown nitride structure was named as 'S-phase'. XRD techniques were then also employed by other researchers to analyse many similar low-temperature nitrided austenitic steels and, mainly according to the results, the unknown nitrogen-supersaturated phase was also called 'expanded austenite' or N-expanded solid solution (γ_N) for its significant lattice expansion as compared to normal austenite in the Fe-Cr-Ni alloys [70,71], or 'm-phase' for the detected tetragonal lattice similar to martensite [72,73].

X-ray diffraction (XRD) has been the mostly used structural

characterization of nitrided austenitic stainless steels since the initial reports of this topic in middle 1980's [24,45,46,61]. In brief, major applications of XRD analyses include the following aspects:

1. Peak broadening indicating intensified lattice distortion in expanded austenite [30,48,55,67,74];
2. Confirmation of the temperature conditions for the formation of single phase expanded austenite[27,34, 36,37,49-52, 56,57,59,67,75];
3. Quantitative measurement of lattice expansion of the new phase, e.g. preferentially more expansion of the (200) plane than other crystal planes [28,35,37,39,48,55-56,74,76,77];
4. Residual stresses arising from the nitrogen super saturation [38,75].

XRD analyses provide structural details of expanded austenite. One typical approach was to study the variation of crystalline parameters at different depths of a nitride surface layer, by acquiring diffraction patterns at a series of electro-polished depth positions [55,77]. It was found that, the (111) diffractions exhibited more pronounced shifting than the (200) diffraction as varying depths. Thus, the expanded austenite was determined to have a face centre tetragonal (f.c.t.) structure, e.g. with estimated lattice dimensions of a=0.393 nm, c=0.380 nm, and c/a=0.965. Interestingly, such f.c.t. structure was not observed on other nitrided surfaces, including other Cr-free austenitic steels in the Fe-Ni and Fe-Mn systems. Similar XRD analyses were also published in [27,38] on several low-temperature nitrided austenitic stainless steels. However, the authors considered the newly formed S-phase to have cubic lattice structure and attributed the tetragonal variation of the cubic lattice to the gradually enhanced residual compressive stresses and stacking defaults. Moreover, Lei also detected XRD and TEM-SAD evidences of strain- and nitrogen-induced h.c.p. martensite $_{N}$ phase in the S-phase layer when the nitriding temperature was as low as 280°C [27].

In Ref [48], the authors found that the XRD peaks of the (200) and (111) planes revealed different values of the lattice expansion, namely 3.9% for (200) plane and 2.3-2.7% for other lattice planes, which were related the estimated nitrogen content of 17.31 at% and 10.37-12.20 at% respectively. The orientation dependent expansion has also been recognised by many other researchers. However, because of the high residual stresses, it was impossible to accurately determine the lattice parameter of the expanded austenite before the work of Christiansen and Somes [78]. In that paper, the investigators applied XRD analysis on two specially prepared powder samples (stress-free) of gas-nitrided austenitic stainless steel AISI 316, and subsequently determined the cubic lattice parameter to be 0.38651 nm and 0.38869 nm respectively for the two samples nitrided at different gas partial pressures. In addition to approving the FCC structure, the XRD work also revealed the effect of stacking faults on the deviations of the XRD line profiles. In Ref. [75], the authors reported comprehensive XRD characterization of an AISI 316L steel nitrided under several temperatures of 350°C, 400°C and 500°C. Considering the overlapping and broadening diffraction peaks, e.g. in the range of the (111) and (200) diffractions of the S-phase, they applied a method of peak de-convolution and predicted possible presence of several nitride phases in the obtained nitrided layers and confirmed the predictions with simultaneous experiments of conversion electron Mossbauer spectroscopy (CEMS). Compared to the lattice parameters of the substrate austenite (a_{γ} = 0.3602 nm) and the iron nitride (a_{Fe4N} = 0.3774 nm), the S-phase showed an expanded parameter a_{S}= 0.3927 nm. Similar to this, the authors in Ref. [79] also confirmed coherent diffraction of CrN nitride within the matrix of S-phase by means of diffraction peak Rietveld refinement and extended X-ray absorption fine structure (EXAFS) analysis.

In Refs. [32,33,65], XRD analyses were employed to investigate the evolution of nitrided structure with increasing time in the 400°C plasma nitriding of the AISI 316L steels. In addition to the pronounced broadening of the (111), (200) and other peaks, the as-measured lattice parameters were found to increase with the nitriding time until it became stabilized after reaching a certain thickness, e.g. after 9~10 hours of nitriding. Very recently, Manova et al. reported in-situ XRD patterns obtained during the ion beam nitriding of austenitic stainless steel AISI 316Ti at a low processing temperature at 400°C for a nitriding times up to 80 minutes [34]. The observed progressive shifting of the (111) and (200) diffraction peaks is consistent to those being observed by other researchers [32,33,61,65].

Structural characterizations by transmission electron microscopy

Transmission electron microscopy (TEM) possesses the most powerful spatial resolution down to nano/atomic scale. TEM is able to show structural features from micro- to nano-scales, such as dislocations, twins and stacking defects, and extremely small volumes of fine precipitates which cannot be detected by other techniques describe above. High resolution TEM has even imaged the ordered distribution of nitrogen interstitial atoms within the anti-phase domains. It also serves as a platform of multi-functional crystallographic, micrographic and chemical analyses. Considering the effect of nitrogen-concentration-dependent S-phase, combined TEM imaging and selected area electron diffraction (SAED) analysis has been applied to determine localised lattice expansion and to recognize the anti-phase domains of ordered nitrogen occupation in the f.c.c. octagonal vacancies. However, a special issue, or an experimental difficulty, is the preparation of thin foil samples for TEM observation. TEM samples of nitrided steels are prepared by ion beam milling, either through back-thinning to obtain a TEM thin foil of the outmost nitride surface, or through cross-sectional thinning to observe structural features across whole depth of a nitride layer, the latter including the latest SEM-based focused ion beam (FIB) thinning.

A typical example of comprehensive TEM studies of low temperature nitrided austenitic stainless steels is the findings of nano-scale anti-phase domains in the single phase of expanded austenite, i.e. through the use of electron diffraction, dark field imaging and high resolution lattice imaging [80,81]. Unlike an ordinary interstitial solid solution phase, selected area diffraction analysis of the the nitrogen-supersaturated austenite showed extra weak diffraction spots in addition to the diffraction spots of the f.c.c. lattice. Then dark field imaging illuminated using a weak diffraction spot showed sub-granular domains and clear boundaries between them. Such anti-phase domains were observed only in the outmost surface region of the nitride depth and disappeared at a depth of 500 nm. The anti-phase domains and anti-phase boundaries were reported to arise from ordered nitrogen distribution in the f.c.c. lattice. Meanwhile, quantitative measurement of the SAD patterns suggested more pronounced lattice expansions in the outmost surface region (5.4%) than the sub-surface region (3.3% at 500 nm sub-surface) as compared to the substrate austenite. Similar short-range ordered domains as well as stacking faults and twins were also observed by Stroz and Psoda in plasma nitride 316L steel [82].

In Ref. [26], the authors reported TEM bright field micrographs and selected area diffraction analysis of an 18Cr-9Ni-Ti austenitic stainless steel plasma nitride at 560°C for five hours. The observed outmost nitride surfaces contained sub-micron scale ferrite grains. In Ref. [27], the same austenitic steel grade was plasma nitriding for four hours at different temperatures in the range 280-480°C. TEM observations confirmed the formation of single f.c.c. γ_{N} phase, with dense dislocations and stacking faults, at the temperature range 300-400°C, free from any nitride precipitates. In contrast, a mixture of disordered f.c.c. γ_{N}, ordered f.c.c. γ'-Fe_4N, and h.c.p. ε'_{N} phase was observed when the steel was nitride

at a lower temperature 280°C. In Ref.[67], the authors compared the structures of nitrided AISI 304 steel being plasma nitride at 400°C and 500°C. Plasma nitriding at 400°C was found to produce a single phase of expanded austenite having dense dislocations and stacking faults. In the sample being nitrided at 500°C, laminated CrN and ferrite structure was observed. In Ref. [48], SAD patterns suggested Cr_2N- and Fe_2N-like fine precipitates in the expanded austenite matrix of 400°C plasma nitrided AISI 304 steel. Similar to this, TEM-SAD analyses were also reported to show the presence of fine carbide or nitride precipitates in plasma ion-treated austenitic steels [31,35,68].

The first results of cross-sectional TEM of plasma nitride austenitic stainless steels were published in Refs. [76,80]. In Ref. [80], a single phase f.c.c. γ_N was confirmed in an austenitic stainless steel being plasma nitride for onehour at 400°C. In another case of similar nitriding, however, Ref [76] showed a 100 nm thick top layer of CrN+ ferrite although the majority of the 1.7 μm thick nitride layer exhibited a single γ_N phase.

So far, the conventional characterizations highlighted above provide extensive understanding of the nitride austenitic stainless steels from general aspects of materials science, i.e. regarding the nitride layer as a homogeneous structure, although limited results of TEM analysis have brought a little insight into their heterogeneous nature. More details of experimental findings on the heterogeneity of low temperature nitride austenitic stainless steels are reviewed below.

Structural characterizations by atomic (magnetic) force microscopy

Magnetic force microscope (MFM) is a special variety of atomic force microscope (AFM), which uses a magnetized stylus to make 2-dimensional scan over an objective surface so that the magnetic structure of the scanned area can be re-constructed at high magnification.

In Ref.[76], the surface of at 400°C plasma nitrided AISI 316 steel, having XRD approved single phase of expanded austenite was analysed by AFM and MFM. Whereas the AFM image showed coarse equaxial grains and parallel slips within every grain, MFM showed that each grain contained tens to hundreds of fine magnetic domains.

Similar MFM analyses of nitride austenitic stainless steel samples were reported in Refs.[74, 83].MFM imaging on polished cross-sections of nitrided steel samples revealed that such sub-grain magnetic domains appeared only in the outer part of a nitride layer, i.e. where the nitrogen supersaturation is higher than the inner part as confirmed by SEM-EDX linear scans. The magnetic domains extended from the outmost nitride surface to certain depth well away from the front of the nitrogen penetration. Ref. [83] measured that the transition from the outer ferromagnetic region to the inner paramagnetic region referred to a nitrogen concentration of approximately 14 at%. In the MFM images shown in Ref.[74], the magnetic domains exhibited elongated cellular patterns within each original austenite grain and the orientations of the domains in nearby grains differ from each other.

By its nature, the contrast in MFM imaging reflects only to the magnetic-field gradient detected in the examined area. The paramagnetic to ferromagnetic transition occurs by two mechanisms, namely, the rearrangement of *3d* electrons after changing FeCrNi atomic distances and the formation of metallic nitrides [36]. In the nitride FeCrNi stainless steel, the induced ferromagnetism implies the dominant Cr-N interaction which removes the Cr *3d* electrons from the metal alloy valence band and leaves ferromagnetic Fe and Ni [83]. Moreover, the magnetic domains observed suggest heterogeneous distribution of the Cr-N bonds inside the nitrided austenite.

Structural-chemical characterization by Mossbauer spectroscopy

Mossbauer spectroscopy is a powerful tool in probing the variation in the local environment of iron atoms in ferrous alloys [84-88]. Accordingly, it is capable of detecting the atomic and electronic interactions between Fe and other alloying elements, such as new phases and short-range ordered clusters existing in a nitrided austenite.

The published papers on Mossbauer spectroscopic analyses of nitride stainless steels have few up to date. In Ref. [89], the authors measured the variation of CEMS patterns of room-temperature ion implanted AISI 304 stainless steel as a function of the introduced ion dose. They found that, the sample treated at a low dose exhibited features from both the paramagnetic austenite substrate and a new phase of interstitial nitrogen sold solution (γ_N-expanded austenite). In contrast, ion implantation at higher dose resulted in the formation of a ferromagnetic compound ε-$Fe_{2+x}N$. In Ref [75], CEMS analysis of a series of AISI 316L stainless steel samples nitrided at temperatures from 350°C to 500°C revealed detailed hyperfine parameters of the resultant structures. Whereas the un-nitrided 316L steel exhibited quadruple splitting and isomer shift parameters of the austenite phase, the nitrided samples showed hyperfine parameters of several phases including both ferromagnetic and paramagnetic expanded austenite γ_N, two types of iron nitrides, and two types of ferrite. In another paper [88], CEMS and convention X-ray Mossbauer spectroscopy (CXMS) were applied to analyse AISI 316 austenitic stainless steel samples subjected to a laser nitriding or carburizing treatment, with the resultant nitrogen content of 8.5 at% and carbon contents of up to 5.8 at% respectively. The spectra revealed three sites for the Fe atoms with different local environments. The hyperfine parameters of Fe-N austenite and Fe-C austenite were strongly dependent on the contents of the interstitial elements and their distributions cannot be unambiguously described with respect to random and ordering modes. The experiment results clearly indicated a weak attractive interaction between the nitrogen interstitials and a stronger repulsive interaction between carbon interstitials.

From these descriptions, however, one may have noticed the drawback of Mossbauer spectroscopy in analysing interactions between nitrogen and the alloying elements of stainless steels other than the base element Fe. For example, CEMS failed to find any evidence of chromium nitride, either in the form of crystalline CrN or as short range ordered clusters or precipitates. Because the coexistence of Fe, Cr and Ni atoms in the same crystal structure, the implanted nitrogen atoms/ions would causes electronic changes in the existing valence configurations and leads to the formation of new bonds or modification of the existing ones.

Chemical analyses by X-ray photo-electron and Auger-electron spectroscopic techniques

XPS and AES have been extensively applied in the chemical compositional and structural analyses of nitride cases. In addition to the determination of nitrogen profiles as mentioned early, XPS serves as a major tool in providing precise separation of the chemical binding energies, e.g., in the determination of chemical bonds existing in a nitride structure.

Lei and Zhu [90] applied AES and XPS to study the expanded austenite phase formed on plasma nitride 18-8 austenitic stainless steel and found that, all the chromium and part of the iron were in the nitride state and all the nickel was in metallic state. As compared to stoichiometric nitrides, the nitrided phase contains weaker Cr-N ionic-type bonds and stronger Fe-N ionic-type bonds. Ref.[91] reported that the main N 1s peak fitting components in a room-temperature plasma nitrided 316 austenitic stainless steel can be described as CrN (396.9 eV) and Cr_2N (397.6 eV).

Furthermore, the development of high energy XPS and AES analyses

provides more informative signals to study the local charge variation of an alloy system. In Ref. [92,93], extensive XPS and AES analyses were undertaken on several Cr-Ni alloyed steels to investigate the local charge variation phenomena taking place at the atomic level, which was claimed to have dominant effect on the local atomic potential. In brief, because of the difference electronegativeness of Cr, Fe and Ni, Cr acts as a cation in the Fe-Cr-Ni system to donate electrons to Fe whereas Ni attracts electrons from Fe. The electron donation and attraction would imply the formation of Fe-Cr and Fe-Ni electric poles, and thus bring about attractive interaction between dissimilar electric poles and the repulsive energy between similar electric poles. Obviously, such fundamental studies help to gain a deeper understanding on the chemical heterogeneity of austenitic stainless steels.

Similar to these, literature [94] and references therein studied the tendency of inter-atomic interactions among Fe, Cr and Ni in the same alloy system. By means of the measurements of conduction electron spin resonance, Gavriljuk et al. concluded that, in substitutional f.c.c. iron-based solid solutions, alloying elements located left of iron in the periodical table, e.g. Cr and Mn, decrease the free electron concentration and promote clustering of solute atoms. On the other hand, alloying elements located right of iron, e.g. Ni and Cu, increase the free electron concentration and assist short range atomic ordering. This paper has been highly cited, but unfortunately, by researchers other than those in the studies of nitride austenitic stainless steels. Nevertheless, the fundamental understanding suggested atomic scale chemical heterogeneity in the FeCrNi alloy system. For example, such extremely fine chromium clustering helps understanding the preferential Cr-N bonding as detected by XPS measurements and partially forms the basis for the Cr-trapping and detrapping dominated nitrogen penetration model.

Other analytical approaches on the chemistry of nitride surfaces

In addition to XPS and AES, there are several other analytical techniques which probe the local chemical environments of alloys, such as extended X-ray absorption fine structure analysis (EXAFS), TEM based electron energy loss spectroscopy (EELS) and energy loss near edge structure (ELNES) analysis. Recently, the present author has employed EELS and ELNES in the characterization of nanocomposite coatings and wear induced tribo-chemical reactions [95-98], which not only demonstrated energy resolution in detecting light elements, like carbon, nitrogen and oxygen, but also evidenced the occurrence of sliding-induced oxidation of the nitrides. Therefore, we expect that EELS or ELNES analysis will be a useful tool in characterization of nitride steels.

EXAFS refers to the details of X-ray absorption by an atom at energies near and above the core-level binding energies, which is sensitive to the changes in the local chemical environments, e.g. the distance, coordination number and species of atoms immediately surrounding the selected element. Oddershede et al. reported EXAFS investigations of short-range atomic orders in nitrided austenitic stainless steel [79, 99]. They found that, N as a nearest neighbour leads to larger distortions of the local environment of Cr than for Ni and Fe. The majority of Cr atoms in the nitride sample was found to be present in Cr-N bond in an environment identical to or reminiscent of CrN nitride, with the EXAFS estimated local lattice constant of 0.412 – 0.413 nm as compared to 0.4148 nm of CrN. The Fe atoms in the expanded austenite experienced a change in chemical surroundings from austenite to iron nitride phases, γ'-Fe_4N_{1-x} and ε-Fe_2N_{1-x}.

Discussion and conclusion remarks

In summary, many microscopic and spectroscopic techniques have contributed to the characterization of nitrided austenitic stainless steels. Up to now, we are able to draw a more detailed sketch of the special structure generated by low temperature nitriding. The special structure, whatever in the name of expanded austenite, S-phase or others, can still be classified as a single crystalline phase having f.c.c.-like lattice type. The so-called single phase is mainly defined according to its XRD- and TEM-related characteristics, such as the crystalline homogeneous without any long-range ordered secondary precipitates, and the presence of dense crystalline defects including supersaturated interstitial nitrogen, dislocations and stacking faults. However, such conventional understanding of crystallography is not enough to describe its enriched physical and chemical nature. Beyond that, the most pronounced feature is, at least up to the frontier of current understanding, that the supersaturated nitrogen atoms do not homogeneously occupy the octagonal vacancies of the f.c.c. Fe-Cr-Ni crystalline lattice. Instead, the nitrogen atoms preferentially form strong ionic bonds to the Cr atoms, whereas the probability to bond to Fe atoms is remarkably smaller and the Ni atoms remain mostly in metallic bonds. In other words, the nitrogen, despite its supersaturation, exhibits a strong heterogeneity in the form of nano-scale 'nitrogen clouds' surrounding Cr atom clusters. In the view of thermodynamics, such Cr-cored 'nitrogen clouds' are in good consistency with the Cr-trapping and de-trapping diffusion mode as promoted by the strong Cr-N ionic bonding and, in thermodynamics, should remain the lowest free energy than a homogeneous distribution in the f.c.c. lattice.A similar phenomenon of gaseous agglomerates in interstitial alloys is the 'Cottrell atmosphere', in which small impurity atoms are trapped within dislocations to minimize the overall strain energy of the whole crystalline system. In a recent APT analysis of super-bainitic steel, such agglomeration of carbon atoms along dislocations has been proved [100].

Moreover, we believe that, the Cr dominated nano-scale heterogeneity already exist in a Fe-Cr-Ni austenitic stainless steel prior to a low-temperature nitriding treatment, because at such low temperature the substitutional element Cr does not have sufficient exciting energy to undergo effective diffusion. The nitriding process only makes the heterogeneity being observed as Cr-N bonded clusters. According to the established knowledge, there should be two types of chromium segregation in the austenitic structure. The first type is associated with dendritic segregation of Cr and Ni during the casting of a steel ingot, in which the Fe-Cr-Ni melt solidifies in a temperature range, instead of at a fixed temperature as the solidification of a pure metal. In the solidification most low-melting-point elements distribute more in the last-solidified inter-dendritic volumes. The second type of heterogeneity exist in an equilibrium Fe-Cr-Ni austenite as a result of the different out shell electronic structures of Cr and Ni atoms to the Fe base metal. A research group in the Ukraine Institute of Metal Physics carried out a series of extensive studies on the correlation between electron structure and short range atomic order in Fe-Cr-Ni austenitic stainless steels. They suggested that, carbide-forming elements (like Cr) decrease the free electron concentration and prefer to form short range clusters of the same component (i.e. Cr-Cr bonds) [86,94,101-103]. On the other hand, non-carbide-forming elements (like Ni) increase the free electron concentration and promote short-range ordering (i.e. Fe-Ni bonds).

The thermal stability of the expanded austenite phase depends almost completely on the mobility of Cr atoms. Repeated experimental research, including those cited in this review, has revealed the importance of relatively low nitriding temperature on the formation of single phase expanded austenite, because in such low temperature, the diffusion of substitutional elements is greatly inhibited. As long as pronounced Cr diffusion occurs, the nano-scale Cr-N clusters will be able to grow, leading to the XRD- and SEM-detectable CrN nitride particles. Meanwhile, the Cr-depleting phases α-Fe and γ-Fe_4N are resulted in the close vicinities of the CrN particles. Such multi-phase structure triggers low corrosion resistance although it may maintain high hardness.

Numerous experimental researches have demonstrated the outstanding hardness property and corrosion resistance of the expanded austenite phase generated in low-temperature nitriding. In the view of modern materials science, the expanded austenite can be classified as a nanocomposite medium consisting of Cr-N clusters dispersed in a Fe-Cr-Ni-N matrix. In particular, the Cr-N clusters are short range ordered ionic compounds having coherent lattice relations to the f.c.c. matrix. Further research interests may lie in the study of the strengthening mechanisms. Because such hardened layer can improve significantly the abrasion resistance of austenitic stainless steel, it is worthwhile to investigate the effect of sliding contact, where both tangential stress and frictional heating are introduced, on the structural evolution. Nano-indentation and cross-sectional TEM are recommended for such purposes [95,96,104,105]. Meanwhile, the nanocomposite structure has been found to exhibit excellent corrosion resistance, which is also beneficial to the long-term performance of some special needs, such as medical implanted parts. Fundamental research should be applied to address the atomic scale interactions between the nano-scale clusters and any applied chemical medium.

References

1. Bordjih K, Jouzeau EY, Mainard D, Payan E, Delagoutte JP, et al. (1996) Evaluation of the effect of three surface treatments on the biocompatibility of 316L stainless steel using human differentiated cells. Biomaterials 17: 491-500.
2. Newson T (2003) Stainless steels for hygienic applications, BSSA Conference-Stainless solutions for a sustainable future. Magna Science Advanture Centre, Sheffield.
3. Buhagiar J, Bell T, Sammons R, Dong HS (2011) Evaluation of the biocompatibility of S-phase layers on medical grade austenitic stainless steels. J Mater Sci-Mater Med 22: 1268-1278.
4. Peckner D, Bernstein IM (1977) Handbook of stainless steels. McGraw-Hill Inc.
5. Beddoes J, Parr JG (1999) Introduction to stainless steels. 3rd edition, ASM International, Materials Park, OH, USA.
6. Lo KH, Shek CH, Lai JKL (2009) Recent developments in stainless steels. Mater SciEng R65: 39-104.
7. Machlet AW (2013) Hardening or treatment of steel, iron, &c. United States Patent 1092925.
8. Pye D (2003) Practical Nitriding and FerriticNitrocarburizing. Reprinted by ASM, USA.
9. Fry A (1924) Process for hardening steel alloys. US Patent 1487554.
10. McQuaid HW, Ketcham WJ (1928) Some Practical Aspects of the Nitriding Process. Reprinted from Trans. ASST, Volume 14.
11. Mittemeijer EJ (2013) Fundamentals of nitriding and nitrocarburizing. In: Dossett J, Totten GE (eds), ASM Handbook, ASM International.
12. Lehrer E (1930) About the iron-hydrogen-ammonia equilibrium. Journal of Applied Electrochemistry and Physical Chemistry 36: 383-392.
13. Guerra V, Galiaskarov E, Loureiro J (2003) Dissociation mechanisms in nitrogen discharges. Chemical Physics Letters 371: 576-591.
14. Berghaus B, Bucek H (1960) Nitriding with electric glow discharge. United States Patent 2946708.
15. Georges J (1999) Nitriding process and nitriding furnace therefor. United States Patent 5989363.
16. Collignon P, Georges J, Kunz C (2012) Active Screen Plasma Nitriding. An Efficient, New Plasma Nitriding Technology.
17. Gavriljuk VG (1996) Nitrogen in iron and steel. ISIJ Int 36: 777-786.
18. Speidal MO (1991) Corrosion science of stainless steels. Proceedings of international conference on stainless steels, Iron and Steel Institute of Japan, Tokyo, 25-35.
19. Mudali UK, Khatak HS, Raj B, Uhlemann M (2004) Surface alloying of nitrogen to improve corrosion resistance of steels and stainless steels. Mater Manuf Process 19: 61-73.
20. Fossati A, Galvenetto E, Bacci T, Borgioli F (2011) Improvement of corrosion resistance of austenitic stainless steels by means of glow-discharge nitriding. Corros Rev 29: 209-221.
21. Simmons JW (1996) Overview: high-nitrogen alloying of stainless steels. Mater SciEng A 207: 159-169.
22. Speidal MO (1989) Properties and applications of high nitrogen steels: austenites and duplex. Proceedings of the 1st international conference on high nitrogen steels (Foct J and Hendry A eds.), The Institute of Metals, London, UK, 92-96.
23. Ningshen S, Mudali UK, Mittal VK, Khatak HS (2007) Semiconducting and passive film properties of nitrogen-containing type 316LN stainless steels. Corros Sci 49: 481-496.
24. Ichii K, Fujimura K, Takase T (1986) Structure of the on-nitrided layer of 18-8 stainless steel. Technical Report Kansai University 27: 135-144.
25. H. Dong (2010) S-phase surface engineering of Fe-Cr, Co-Cr and Ni-Cr alloys. Int Mater Rev 55: 65-98.
26. Li J, Yuan Y, Yuan KQ (1991) Alpha-phase microcrystalline structure if ion nitride layer on steels. ActaMetall Sin 27: B368-B370.
27. Lei MK (1999) Phase transformation in plasma source ion nitride austenitic stainless steel at low temperature. J Mater Sci 34: 5975-5982.
28. Wu D, Kahn H, Dalton JC, Michal GM, Ernst F, et al. (2014) Orientation dependence of nitrogen supersaturation in austenitic stainless steel during low-temperature gas phase nitriding. Acta Mater 79: 339-350.
29. Sun Y (2010) Production of nitrogen and carbon S phases in austenitic stainless steels by hybrid plasma surface alloying. Surf Eng 26: 114-122.
30. Zhao C, Sun DG (2004) Plasma nitrocarburising of austenitic stainless steel at low temperature. J Qingdao UnivSciTechnol 25: 238-241.
31. Buhagiar J, Li XY, Dong HS (2009) Formation and microstructual characterization of S phase layers in Ni-free austenitic stainless steels by low-temperature plasma alloying. Surf Coat Technol 204: 330-335.
32. Templier C, Stinville JC, Villechaise P, Renault PO, Abrasonis G, et al. (2010) On lattice plane rotation and crystallographic structure of the expanded austenite in plasma nitride AISI 316L steel, Surf Coat Technol 204: 2551-2558.
33. Moskalioviene T, Galdikas A, Riviere JP, Pichon L (2011) Modeling of nitrogen penetration in polycrystalline AISI 316L austenitic stainless steel during plasma nitriding. Surf Coat Technol 205: 3301-3306.
34. Manova D, Mandl S, Neumann H, Rauschenbach B (2014) Analysis of in situ XRD measurements for low energy ion beam nitriding of austenitic stainless steel. Surf Coat Technol 256: 64-72.
35. Dalibon EL, Bozzano PB, Bruhl SP (2013) Microstructure of nitride layer in AISI 316L stainless steel after low temperature ion nitriding. Acta Microscopica 22: 4-11.
36. Martinavicius A, Abrasonis G, Scheinost AC, Danoix R, Danoix F, et al. (2012) Nitrogen interstitial diffusion induced decomposition in AISI 304L austenitic stainless steel. Acta Mater 60: 4065-4076.
37. Asgari M, Barnoush A, Johnsen R, Hoel R (2011) Microstructural characterization of pulsed plasma nitrided 316L stainless steel. Mater Sci EnG A 529: 425-434.
38. Sun Y, Li XY, Bell T (1999) X-ray diffraction characterization of low temperature plasma nitride austenitic stainless steels. J Mater Sci 34: 4793-4802.
39. Tsujimura H, Goto T, Ito Y (2004) Growth kinetics of nitride layers on stainless steels durinh electrochemical nitriding in molten LiCl-KCl-Li_3N systems. J New Mater Electrochem Systems 7: 221-230.

40. Pan JS, Tong JM, Tian MB (1998) Fundamentals of Materials Science. Tsinghua University Press, Beijing, 463.

41. Mandl S, Rauschenbach B (2002) Concentration dependent nitrogen diffusion coefficient in expanded austenite formed by ion implantation. J App Phys 91: 9737-9742.

42. Christiansen T, Somers MAJ (2008) Determination of the concentration dependent diffusion coefficient of nitrogen in expanded austenite. Int J Mater Res 99: 999-1005.

43. Parascandola S, Moller W, Willaimson DL (2000) The nitrogen transport in austenitic stainless steel at moderate temperature. Appl Phys Lett 76: 2194-2196.

44. Moller W, Parascandola S, Telbizoiva T, Gunzel R, Richter E (2001) Surface processes and diffusion mechanisms of ion nitriding of stainless steel and aluminium. Surf Coat Technol 136: 73-79.

45. Zhang ZL, Bell T (1985) Structure and corrosion resistance of plasma nitride stainless steel. Surf Eng 1: 131-136.

46. Rolinski E (1987) Effect of plasma nitriding temperature on surface properties of austenitic stainless steel. Surf Eng 3: 35-40.

47. Martinavicius A, Danoix R, Drouet M, Templier C, Hannoyer, et al. (2015) Atom probe tomography characterization of nitrogen induced decomposition in low temperature plasma nitride 304L austenitic stainless steel. Mater Lett 139: 153-156.

48. Pedraza F, Grosseau-Poussard JL, Abrasonis G, Riviere JP, Dinhut JF (2003) Influence of low energy high fluc nitrogen implantation on the oxidation behaviour of AISI 304L austenitic stainless steel. J Appl Phys 94: 7509-7520.

49. Fossati A, Borgioli F, Galvanetto E, Bacci T (2006) Corrosion resistance properties of glow-discharge nitrided AISI 316L austenitic stainless steel in NaCl solutions. Corr Sci 48: 1513-1527.

50. Li GJ, Peng Q, Li C, Wang Y, Gao J, et al. (2008) Effect of DC plasma nitriding temperature on microstructure and dry-sliding wear properties of 316L stainless steel. Surf Coat Technol 202: 2749-2754.

51. Li Y, Wang L, Xu J, Zhang D (2012) Plasma nitriding of AISI 316L austenitic stainless steels at anodic potential. Surf Coat Technol 206: 2430-2437.

52. Borgioli F, Fossati A, Matassini G, Galvenetto E, Bacci T (2010) Low temperature glow-discharge nitriding of a low nickel austenitic stainless steel. Surf Coat Technol 204: 3410-3417.

53. Stinville JC, Tromas C, Villechaise P, Templier C (2011) Anisotropy changes in hardness and indentation molulus induced by plasma nitriding of 316L polycrystalline stainless steel. Script Mater 64: 37-40.

54. Tromas C, Stinville JC, Templier C, Villechaise P (2012) Hardness and elastic modulus gradients in plasma nitrided 316L polycrystalline stainless steel investigated by nanoindentation tomography. Acta Mater 60: 1965-1973.

55. Yasumaru N (1998) Low-temperature ion nirriding of austenitic stainless steels. Mater Trans JIM 39: 1046-1052.

56. Singh V, Marchev K, Cooper CV, Meletis EI (2002) Intensified plasma-assisted nitriding of AISI 316L stainless steel. Surf Coat Technol 160: 249-258.

57. Wang J, Xiong J, Peng Q, Fan H, Wang Y, et al. (2009) Effect of DC plasma nitriding parameters on microstructure and properties of 304L stainless steel. Mater Characterization 60: 197-203.

58. Takahashi T, Burghaus J, Music D, Dronskowski R, Schneider JM (2012) Elastic properties of γ'-Fe_4N probed by nanoindentation and ab initio calculation. Acta Mater 60: 2054-2060.

59. Wang L, Xu XL, Xu B, Yu ZW, Hei ZK (2000) Structure and wear resistance of ion nitride austenite stainless steel. Tribology 20: 67-69.

60. Li Y, Zhang SZ, He YY, Zhang L, Wang L (2014) Charactistics of the nitrided layer formed on AISI 304 austenitic stainless steel by high temperature nitriding assisted hollow cathode discharge. Mater Design 64: 527-534.

61. Li Y, Wang Z, Wang L (2014) Surface properties of nitride layer on AISI 316L austenitic stainless steel produced by high temperature plasma nitriding in short time. Appl Surf Sci 298: 243-250.

62. Toshkov V, Russev R, Madjarov T, Russeva E (2007) On low temperature ion nitriding of austenitic stainless steel AISI 316. J Achievements Mater Manuf Eng 25: 71-74.

63. Borgioli F, Fossati A, Galvenetto E, Bacci T (2005) Glow-discharge nitriding of AISI 316L austenitic stainless steel: influence of treatment temperature. Surf Coat Technol 200: 2474-2480.

64. Ozturk O, Okur S, Riviere JP (2009) Structural and magnetic characterization of plasma ion nitrided layer on 316L stainless steel alloy. Nucl Instrum Methods Phys Res B 267: 1540-1545.

65. Stinville JC, Villechaise P, Templier C, Riviere JP, Drouet M (2010) Plasma nitriding of 316L austenitic stainless steel: Experimental investigation of fatigue life and surface evolution. Surf Coat Technol 204: 1947-1951.

66. Gallo AC, Dong H (2012) New insights into the mechanism of low temperature active screen plasma nitriding of austenitic stainless steel. Script Mater 67: 89-91.

67. Xu XL, Wang L, Yu ZW, Hei ZK (2000) Microstructural characterization of plasma nitrided austenitic stainless steel. Surf Coat Technol 132: 270-274.

68. Li W, Li XY, Dong H (2011) Effect of tensile stress on the formation of S-phase during low-temperature plasma carburizing of 316L foil. Acta Mater 59: 5765-5774.

69. Prandel LV, Somer A, Assmann A, Camelotti F, Costa G, et al. (2013) Plasma nitriding process by direct current glow discharge at low temperature increasing the thermal diffusivity of AISI 304 stainless steel. J Appl Phys 113: 063507.

70. Leyland A, Lewis DB, Stenenson PR, Matthews A (1993) Low temperature plasma diffusion treatment of stainless steels for improved wear resistance. Surf Coat Technol 62: 608-617.

71. Williamson DL, Ozturk O, Wei R, Wilbur PJ (1994) Metastable phase formation and enhanced diffusion in f.c.c. alloys under dose, high flux nitrogen implantation at high and low ion energies. Surf Coat Technol 64: 15-23.

72. Yasumaru N, Kamachi K (1986) Nitrogen induced transformation in type 304 austenitic stainless steel. J Japen Inst Metals 50: 362-368.

73. Marchev K, Cooper CV, Blucher JT, Giessen BC (1998) Conditions for the formation of a martensitic single-phase compound layer in ion-nitrided 316L austenitic stainless steel. Surf Coat Technol 99: 225-228.

74. Öztürk O, Fidan M, Mandl S (2014) MFM imaging of expanded austenitic formed on 304 SS and CoCrMo alloys. Surf Coat Technol 256: 15-22.

75. Gontijo LC, Machado R, Miola EJ, Casteletti LC, Alcantara NG, et al. (2006) Study of the S phase formed on plasma-nitrided AISI 316L stainless steel. Mater Sci Eng A 431: 315-321.

76. Fewell MP, Mitchell DRG, Priest JM, Short KT, Collins GA (2000) The nature of expanded austenite. Surf Coat Technol 131: 300-306.

77. Li Y, Wang L (2014) Research progress in plasma nitriding. Materials Review 28: 61-64.

78. Christiansen T, Somers MAJ (2004) On the crystallographic structure of S-phase. Scr Mater 50: 35-37.

79. Oddershede J, Christiansen TL, Stahl K, Somers MAJ (2008) EXAFS investigation of low temperature nitride stainless steel. J Mater Sci 43: 5358-5367.

80. Jiang JC, Meletsi EI (2000) Microstructure of the nitrid layer of AISI 316 stainless steel produced by intensified plasma assisted processing. J Appl Phys 88: 4026-4032.

81. Meletis EI, Singh V, Jiang JC (2002) On the single phase formed during low-temperature plasma nitriding of austenitic stainless steels. J Mater Sci Lett 21: 1171-1174.

82. Stroz D, Psoda M (2010) TEM studies of plasma nitride austenitic stainless steel. J Microsc 237: 227-231.

83. Basso RLO, Pimentel VL, Weber S, Marcos G, Czerwiec T, et al. (2009) Magnetic and structural properties of ion nitride stainless steel. J Appl Phys 105: 124914.

84. Oda K, Umezu K, Ino H (1990) Interaction and arrangement of nitrogen atoms in FCC gamma-iron. J Phys Condens Matter 2: 10147-10158.

85. Nadutov VM (1998) Mossbauer analysis of the effect of substitutional atoms on the electron charge distribution in nitrogen and carbon austenites. Mater Sci Eng A 254: 234-241.

86. Shanina BD, Gavriljuk VG, Konchits AA, Kolesnik SP (1998) The influence of substitutional atoms upon the electron structure of the ion-based transition metal alloys. J Phys Conden Matter 10: 1825-1838.

87. Desimoni J (2004) Arrangements of interstitial atoms in *fcc* Fe-C and Fe-N solid solutions. In: Elzain ME, Yousif AA, Al Rawas AD, Gismelseed AM (eds) ICAME 2003: 505-521.

88. Binczycka H, Kahle M, Cusenza S, Carpene E, Schaaf P (2006) Interstitial ordering of nitrogen and carbon in laser nitride and laser carburized austenitic stainless steel. J Phys Condens Matter 18: 10561-10570.

89. Briglia T, Terwagne G, Quaeyhaegens C, H'Haen J, Stals LM (1996) Study of nitrogen implanted stainless steels by CEMS and TEM. Surf Coat Technol 80: 105-108.

90. Lei MK, Zhu XM (2004) Chemical state of nitrogen in a high nitrogen face-centred-cubic phase formed on plasma source ion nitride austenitic stainless steel. J Vac Sci Technol 22: 2067-2070.

91. Meskinis S, Andrulevicius M, Kopustinskas V, Tamulevicius S (2005) XPS study of the ultrathin a-C:H films deposited onto ion beam nitride AISI 316 steel. Appl Surf Sci 249: 295-302.

92. Moslemzadeh N, Beamson G, Diplas S, Tsakiropoulos P, Watts JF (2008) Monitoring atomic level electronic changes in the alloying of stainless steels with Auger and photoelectron spectroscopy. Surf Sci 602: 216-225.

93. Diplas S, Moslemzadeh N, Watts JF, Beamson G, Tsakiropoulos P (2010) An XPS study of the interatomic charge distribution in stainless steels. Surface and Interface Analysis 42: 722-725.

94. Gavriljuk VG, Shanina BD, Berns H (2000) ON the correlation between electron structure and short range atomic order in iron-based alloys. Acta Mater 48: 3879-3893.

95. Luo Q, Hovsepian PE (2006) Transmission electron microscopy and energy dispersive X-ray spectroscopy on the worn surface of nano-structured TiAlN/VN multilayer coating. Thin Solid Films 497: 203-209.

96. Luo Q, Zhou Z, Rainforth WM, Bolton M (2009) Effect of tribofilm formation on the dry sliding friction and wear properties of magnetron sputtered TiAlCrYN coatings. Tribo Lett 34: 113-124.

97. Luo Q, Zhou Z, Rainforth WM, Hovsepian PE (2006) TEM-EELS study of low-friction super-lattice TiAlN/VN coating: The wear mechanisms. Tribo Lett 24: 171-178.

98. Luo Q, Wang SC, Zhou Z, Chen L (2011) Structure characterization and tribological study of magnetron sputtered nanocompositenc-TiAlV(N, C)/a-C coatings. J Mater Chem 21: 9746 - 9756.

99. Oddershede J, Christiansen TL, Stahl K, Somers MAJ (2010) Extended X-ray absorption fine structure investigation of nitrogen stabilized expanded austenite. Scrip Mater 62: 290-293.

100. Caballero FG, Miller MK, Babu SS, Garcia-Mateo C (2007) Atomic scale observations of bainite transformation in a high carbon high silicon steel. Acta Mater 55: 381-390.

101. Gavriljuk VG, Shanina BD, Berns H (2008) A Physical concept for alloying steels with carbon+nitrogen. Mater Sci Eng A 481-482: 707-712.

102. Petrov YN (2005) On the electron structure of Mn-, Ni- and Cr-Ni-Mn austenite with different stacking fault energy. Script Mater 53: 1201-1206.

103. Shanina BD, Tyshchenko AI, Glavatskyy IN, Runov VV, Petroc YN, et al. (2011) Chemical nano-scale homogeneity of austenitic CrMnCN steels in relation to electronic and magnetic properties. J Mater Sci 46: 7725-7736.

104. Luo Q, Rainforth WM, Münz WD (1999) TEM observation of wear mechanisms of TiAlCrN and TiAlN/CrN coatings. Wear 225-229: 74-82.

105. Luo Q, Rainforth WM, Münz WD (2001) TEM study of the wear of TiAlN/CrN superlattice coatings. Scr Mater 45: 399-404.